

A novel active contour for medical image segmentation

Mahdi Saadatmand-Tarjzan and Hassan Ghassemian^{a)}

School of Electrical and Computer Engineering, Tarbiat Modares University, Tehran, Iran

a) ghassemi@modares.ac.ir

Abstract: In this paper, a novel parametric active contour is proposed for image segmentation. It integrates the wavelet transform and self-affine mapping system to effectively compute the external force of parametric active contours. For this purpose, after smoothing the image by a Gaussian kernel, the wavelet coefficients are computed. Then, sub-forces of each wavelet scale were computed by using contractive self-affine maps. Finally, the total self-affine force field was obtained by superposition of these sub-forces. Experimental results demonstrated the superior performance of the proposed algorithm compared to a number of frequently-used active contours for medical images.

Keywords: active contours, wavelet transform, self-affine mapping system, medical image segmentation

Classification: Science and engineering for electronics

References

- [1] A. Fernández-Caballero and J. M. Vega-Riesco, “Determining heart parameters through left ventricular automatic segmentation for heart disease diagnosis,” *Expert Systems with Applications*, vol. 36, pp. 2234–2249, 2009.
- [2] C. D. Garson, B. Li, S. T. Acton, and J. A. Hossack, “Guiding automated left ventricular chamber segmentation in cardiac imaging using the concept of conserved myocardial volume,” *Computerized Medical Imaging and Graphics*, vol. 32, pp. 321–330, 2008.
- [3] C. Xu, D. Pham, and J. L. Prince, “Image segmentation using deformable models,” In J. Fitzpatrick and M. Sonka (editors), *Handbook of Medical Imaging, vol. 2: Medical Image Proc. and Analysis*, pp. 175–272, 2000.
- [4] C. Xu and J. L. Prince, “Snakes, shapes, and gradient vector flow,” *IEEE Trans. Image Process.*, vol. 7, no. 3, pp. 359–369, 1998.
- [5] C. Xu and J. L. Prince, “Generalized gradient vector flow external forces for active contours,” *Signal Process.*, vol. 71, pp. 131–139, 1998.
- [6] T. F. Chan and L. A. Vese, “Active contours without edges,” *IEEE Trans. Image Process.*, vol. 10, no. 2, pp. 266–277, 2001.
- [7] N. Paragios and R. Deriche, “Geodesic active regions: a new paradigm to deal with frame partition problems in computer vision,” *J. Visual Commun. Image Representation.*, vol. 13, no. 1-2, pp. 249–268, 2002.
- [8] C. Li, C.-Y. Kao, J. C. Gore, and Z. Ding, “Minimization of region-scalable fitting energy for image segmentation,” *IEEE Trans. Image Process.*, vol. 17, no. 10, pp. 1940–1949, 2008.

- [9] M. Saadatmand-Tarzjan and H. Ghassemian, “Self-affine snake: a new parametric active contour,” *IEEE Int. Conf. Signal Process. Commun.*, pp. 492–495, Nov. 2007.
- [10] T. Ida and Y. Sambonsugi, “Self-affine mapping system and its application to object contour extraction,” *IEEE Trans. Image Process.*, vol. 9, no. 11, pp. 1926–1936, 2000.
- [11] M. Saadatmand-Tarzjan and H. Ghassemian, “On analytical study of the self-affine mapping system in the image processing domain,” *17th Iranian Conference Electrical Engineering (ICEE 2009)*, 2009.
[Online] http://saadatmand.synthasite.com/resources/Conf0034_Full.pdf
- [12] S. Mallat, *A Wavelet Tour of Signal Processing*, 2nd ed., Academic Press, 1999.
- [13] I. Daubechies, *Ten lectures on wavelets CBMS, SIAM*, vol. 61, p. 271, 1994.

1 Introduction

Although segmented medical images are used routinely in a multitude of different applications, medical image segmentation remains a difficult task due to both tremendous variability of tissue shapes and variation in the image quality [1, 2, 3]. In general, medical images are usually corrupted by noise, sampling artifacts, and edge uncertainty. Active contours or snakes have been introduced as a solution.

Generally speaking, active contours are deformable models which can deform/evolve in the image domain in order to minimize internal and external energies. The traditional snakes (referred to as edge-based active contours) may provide unacceptable results for medical images due to using poor gradient-based forces [2, 4, 5]. To tackle this problem, some researchers used *a priori* information to improve the performance of the snake [1] while other ones proposed region-based active contours (RBACs) [6]. Although RBACs provided promising results, they may decline boundary localization performance. To address this disadvantage, some researchers tried to integrate the edge and region-based models [7]. Recently, patch-based RBACs are proposed to improve the performance of snakes for images with texture, intensity in-homogeneity, noise corruption, or heterogeneous objects [8].

In this paper, we proposed self-affine snake (SAS) by integrating wavelet transform and self-affine mapping system (SAMSYS) to provide external forces of parametric active contours. Indeed, the proposed snake uses a patch-based method to compute edge-based self-affine external forces [9]. Experimental results demonstrated the remarkable performance of SAS compared to four well-known active contours including balloon [3], gradient vector flow (GVF) [4], generalized GVF (GGVF) [5], and Chan-Vese’s geodesic active contour (CV) [6].

2 Self-affine mapping system

Consider an image having the domain $\Omega \subset R^2$ with the intensity $I(\mathbf{x}) \in [0, 1]$ for all $\mathbf{x} = (x, y) \in \Omega$. The contractive self-affine map (CSAM) $m_p: M_p \rightarrow W_p$ attached to the component $\mathbf{p} = (p, q)$ is defined as follows:

$$m_p(\mathbf{x}) = r(\mathbf{x} - \mathbf{p}) + \boldsymbol{\tau}_p + \mathbf{p}, \quad r < 1 \quad (1)$$

where r is the scaling coefficient and $\boldsymbol{\tau}_p = (s_p, t_p)$ is the translation vector (TV) which points from the center point of the domain-patch M_p (i.e. \mathbf{p}) toward the center point of the range-patch W_p (i.e. $\mathbf{q} = \boldsymbol{\tau}_p + \mathbf{p}$). Indeed, this equation translates M_p by $\boldsymbol{\tau}_p$ and contracts it by r to make W_p . To optimize $\boldsymbol{\tau}_p$, in each step of the matching algorithm, the value of one parameter is changed and the following cost function is evaluated:

$$e(\boldsymbol{\tau}_p) = \frac{1}{2} \iint_{x \in M_p} (I(\mathbf{x}) - I(m_p(\mathbf{x})))^2 dx dy \quad (2)$$

After checking all possible situations, the globally optimal TV (GOTV) is determined by the best TV with the smallest cost value.

Ida and Sambonsugi showed that each component of the image, after mapping by a CSAM, approaches toward an image edge. They used this property to provide a contour extraction algorithm [10]. Obviously, \mathbf{p} is usually mapped to \mathbf{q} , i.e. $\mathbf{q} = m_p(\mathbf{p})$. Therefore, each GOTV (i.e. $\boldsymbol{\tau}_p$) should point toward an image corner or edge within the domain-patch [11]. The proposed self-affine forces are computed based on this important property which is referred to as the corner/edge pointing (CEP) behavior.

3 Self-affine snake

The proposed active contour consists of six steps: *i*) smoothing the input image, *ii*) computing wavelet coefficients, *iii*) extracting self-affine maps, *iv*) computing sub-forces of each wavelet scale, *iv*) combining sub-forces of different scales to make self-affine forces, and *v*) snake convergence using the resultant forces.

In more detail, the given image is initially smoothed by using the Gaussian kernel $G_{\sigma_{SAS}}$ with the standard deviation (STD) of σ_{SAS} to suppress noise. Then, wavelet coefficients of the resultant image are computed in n consecutive scales by using Mallat's orthogonal wavelet decomposition algorithm [12]. For this purpose, the biorthogonal spline wavelet transform is employed because of symmetry, compactness, and exact reconstruction with FIR filters [13].

After that, for the component \mathbf{p}^m of the matrix LL of the m -th wavelet scale, a CSAM is defined by assigning a disk-shaped domain-patch (thanks to symmetry in all directions) centered at \mathbf{p}^m with the radius of μ pixels. The optimal GOTV (i.e. $\boldsymbol{\tau}_p^m$) of this CSAM is obtained by the matching algorithm stated in Section 2.

According to the CEP behavior, every GOTV points toward a corner/edge within the domain-patch. In more detail, $\boldsymbol{\tau}_p^m$ is zero once the center of the

domain-patch is located on the desirable boundary; and otherwise, it offers a suitable direction to move the active contour at \mathbf{p}^m . Besides, the length of τ_p^m depends on the distance between \mathbf{p}^m and the corner/edge. Also, in order to provide a robust convergence performance, the external force should be increased by approaching toward the desirable boundary. Thus, we experimentally investigated the following formula to compute sub-forces of the m -th wavelet scale:

$$\mathbf{f}^m(\mathbf{p}^m) = \frac{\tau_p^m}{(1 + \|\tau_p^m\|)^2} \quad (3)$$

In this equation, $\|\mathbf{f}^m\|$ is decreased by increasing $\|\tau_p^m\|$ while the strongest sub-force is obtained for $\|\tau_p^m\| = 1$. It means that stronger sub-forces are given by closer components to the desired boundary and vice versa. Eq. (3) employs no gradient-based quantity for computing sub-forces therefore; it seems to be significantly robust against noise.

Next, we should effectively combine corresponding sub-forces of different wavelet scales to compute self-affine forces. Details can be found in lower wavelet scales while higher wavelet scales include global information. In other words, low-scale sub-forces are proper for precise fitting while high-scale sub-forces are appropriate to move the active contour toward the object boundary from a far distance. Thus, the former should be weighted by larger scaling coefficients compared to the later as follows:

$$\mathbf{f}_{\text{SAS}}(\mathbf{p}) = \mathbf{f}_{\text{SG}}(\mathbf{p}) + \sum_{m=1}^n \eta^{-m} \mathbf{f}^m\left(\frac{\mathbf{p}}{\eta^m}\right) \quad (4)$$

where $\mathbf{f}_{\text{SAS}}(\mathbf{p})$ indicates the self-affine force at the component \mathbf{p} of the image, η is the scaling coefficient of the wavelet decomposition method (here, $\eta = 2$), and \mathbf{f}_{SG} determines a sub-set of Gaussian forces given by:

$$\mathbf{f}_{\text{SG}}(\mathbf{p}) = \begin{cases} \frac{\mathbf{f}_{\text{G}}(\mathbf{p})}{\max\|\mathbf{f}_{\text{G}}(\mathbf{p})\|} & \frac{\|\mathbf{f}_{\text{G}}(\mathbf{p})\|}{\max\|\mathbf{f}_{\text{G}}(\mathbf{p})\|} > \theta \\ 0 & \text{Otherwise} \end{cases} \quad (5)$$

where \mathbf{f}_{G} is the potential Gaussian force defined as follows:

$$\mathbf{f}_{\text{G}}(\mathbf{p}) = -\nabla \left(\|\nabla [G_{\sigma_{\text{SAS}}} * I(\mathbf{p})]\|^2 \right) \quad (6)$$

Finally, self-affine forces are used to deform the active contour based on the dynamic force formulation [4] as follows:

$$\mathbf{x}_t(s, t) = \alpha \mathbf{x}^{(2)}(s) - \beta \mathbf{x}^{(4)}(s) + \mathbf{f}_{\text{SAS}} \quad (7)$$

where $\mathbf{x}(s) = [x(s), y(s)]$ ($s \in [0, 1]$) is the parametric curve which should be deformed to fit to the desired curve; and α and β control the snake tension and rigidity, respectively. Besides, $\mathbf{x}^{(k)}$ indicates the k -th order derivative of \mathbf{x} with respect to the curve-length parameter (s) and \mathbf{x}_t is the first-order derivative of \mathbf{x} with respect to time (t). Here, when \mathbf{x} stabilizes, the term \mathbf{x}_t vanishes and the snake converges to the resultant curve.

Furthermore, according to Eq. (4), by augmenting the number of wavelet scales (n), the capture range of self-affine forces is increased. Generally, the

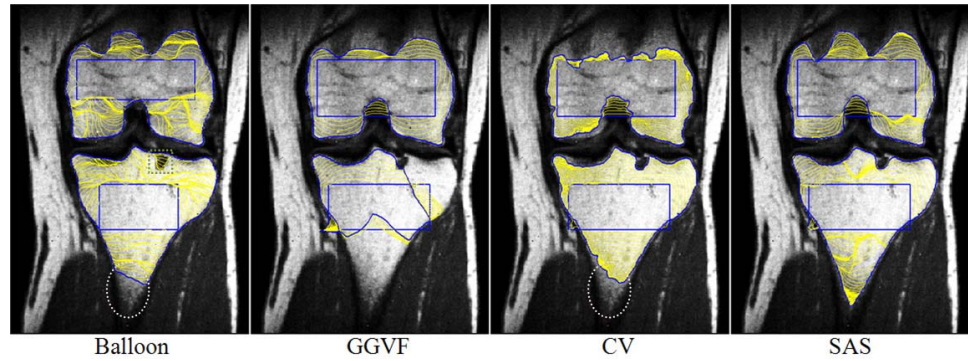


Fig. 1. The results of SAS and three counterpart snakes for the knee image.

Table I. The solution qualities of GVF, GGVF, CV, and SAS for four cardiac MR images.

Image	Size	GVF			GGVF			CV			SAS		
		ψ_{mx}	ψ_{av}	σ_{ψ}	ψ_{mx}	ψ_{av}	σ_{ψ}	ψ_{mx}	ψ_{av}	σ_{ψ}	ψ_{mx}	ψ_{av}	σ_{ψ}
Heart1	128×128	3.2	1.3	0.6	3.7	1.3	0.7	2.5	1.0	0.6	2.5	1.0	0.5
Heart2	128×128	2.5	1.1	0.5	2.4	1.1	0.5	2.8	1.0	0.5	2.4	0.9	0.5
Heart3	128×128	2.8	1.2	0.6	2.5	1.2	0.5	2.5	1.0	0.5	2.4	0.8	0.4
Heart4	128×128	2.9	1.1	0.6	2.0	1.0	0.5	2.4	0.9	0.5	1.9	0.8	0.4
Average		2.9	1.2	0.6	2.7	1.2	0.6	2.6	1.0	0.5	2.3	0.9	0.5

number of required wavelet scales for capturing the snake from the distance d in an image of size $m \times m$ can be simply given by:

$$d \leq \eta^n \times \mu \leq m \Rightarrow \log_{\eta} \left(\frac{d}{\mu} \right) \leq n \leq \log_{\eta} \left(\frac{m}{\mu} \right) \quad (8)$$

Note that SAS can be efficiently implemented by computing self-affine forces only for the components on the current curve in each step of snake deformation.

4 Experimental results

Self-affine snake was compared to four frequently-used active contours including balloon [3], GVF [4], GGVF [5], and CV [6] by using a number of medical images. All experimental results were obtained by an INTEL CORE 2 DUO 2.0-GHz LAPTOP with 1.0-GB main memory using MATLAB environment.

Self-affine snake contains a number of parameters including μ , r , σ_{SAS} , n , θ , α , and β which should be regulated to improve the algorithm performance. We experimentally adjusted μ and r to 5 and 0.5, respectively. Furthermore, in each experiment, the same values of α and β are used for all snakes (*e.g.* $\alpha = \beta = 1$). However, σ_{SAS} , n , and θ should be separately regulated for each image.

Fig. 1 illustrates the results of SAS and three specified snakes for a coronal MR image of the human knee of size 390×290 . Two initial curves were used to separately segment the femoral condyles (superior) and tibia (inferior) in the image while both suffered from non-uniform illumination, noise corruption, and edge uncertainty. All specified snakes except SAS ($\sigma_{SAS} = 2.0$,

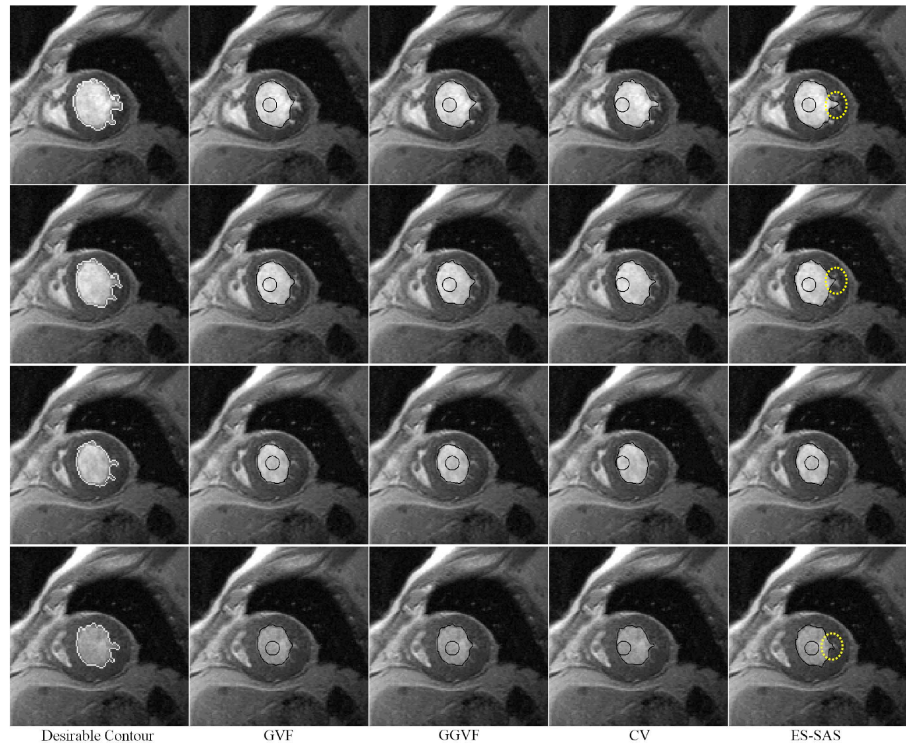


Fig. 2. The results of SAS, GVF, GGVF, and CV compared to the desirable contour for Heart1 to Heart4 arranged from top to bottom.

$n = 6, \theta = 0.2$) failed. In more detail, for the femoral condyles (FC), balloon was successful by using a smaller initial rectangle (quite within the object); otherwise, it stepped out of the desirable boundary due to using unidirectional pressure forces. GGVF and also CV could not converge to the upper boundaries of FC because of noise corruption. Furthermore, for the tibia, both CV and balloon failed to segment the lower corner (indicated by the dotted ellipses). Also, balloon marched over upper indentation determined by the dotted square while GGVF did not provide wide-enough capture range. Besides, for both the initial curves, the CPU times of SAS ($t_{SAS} = 3.1$ and 3.6) is better than those of GGVF ($t_{GVF} = 6.1$ and 5.4) and CV ($t_{CV} = 22.8$ and 35.4) while it took the shortest CPU time for balloon ($t_{BLN} = 2.0$ and 1.5).

In order to further study the above consequences, next experiments were performed on four cardiac MR images of the human heart (referred to as Heart1 to Heart4) to segment the left ventricle. They belonged to the same cardiac cycle. Besides, an expert radiologist accurately indicated the desirable boundary in each image to evaluate the solution quality of every snake based on the fitting and radial error measures [5]. Since they usually provided equivalent results, only fitting errors have been reported in Table I. According to the definition, after convergence of a snake, the fitting error of each curve component was computed as the minimum Euclidean distance to the desirable boundary. Then, the solution quality of the resultant curve can be obtained by computing the average (ψ_{av}), maximum (ψ_{mx}), and STD

(σ_ψ) of all components fitting errors.

Furthermore, all of the snakes except CV used the same initial contour in the center of the left ventricle. CV should be initialized next to the ventricle border; otherwise, it shrinks in the center of the image and fails to converge. Thus, we initialized CV by using a circle near to the left border of the ventricle. According to Table I, the best results were given by SAS. Besides, as further illustrated in Fig. 2, ES-SAS could more accurately fit the curve to the desirable contour compared to CV, GGVF, and GVF (in an ordered manner); especially in boundary indentations (see the dotted ellipses).

The remarkable advantages such as robustness against noise and intensity inhomogeneity, wide capture range, progressing into boundary concavities, and short CPU time introduce SAS as an appropriate approach for segmentation of medical images which are usually corrupted by noise and include uncertain edges.

5 Conclusion

In this paper, self-affine snake was proposed based on the CEP behavior of CSAMs. It effectively integrates the wavelet transform, SAMSYS, and snake model to keep their strengths and avoid the weak points. Experimental results demonstrated remarkable performance for medical image segmentation.